ASTRONOMY AND ASTROPHYSICS

High rotation measure in the steep spectrum quasar 3C 147

R.D. Nan[1], H.Y. Zhang[2,1], D.C. Gabuzda[3,4], J.S. Ping[2], R.T. Schilizzi[3,5], W.W. Tian[1], and M. Inoue[6]

[1] Beijing Astronomical Observatory, National Astronomical Observatories, Chinese Academy of Sciences, A20 Datun Road, Chaoyang District, Beijing 100012, P.R. China
[2] Astronomy Department, Beijing Normal University, Beijing 100875, P.R. China
[3] Joint Institute for VLBI in Europe, Postbus 2, 7990 AA Dwingeloo, The Netherlands
[4] Astro Space Center, Lebedev Physical Institute, 53 Leninskii pr., 117924 Moscow, Russia
[5] Leiden Observatory, Postbus 9513, 2300 RA Leiden, The Netherlands
[6] National Astronomical Observatory, Osawa 2-21-1, Mitaka, Tokyo 181-8588, Japan

Received 29 December 1999 / Accepted 3 April 2000

Abstract. We present VLBA polarimetric observations of the steep-spectrum quasar 3C 147 (0538+498) made at four frequencies in the available 5-GHz band, from which we derived milliarcsecond-resolution images of the total intensity, polarization, and rotation measure distributions. The jet extending to the southwest is followed out to a distance of about 200 mas from the core. The jet shows several gentle wiggles, and turns sharply toward the north near the end of its detected length. Polarization was detected in one bright feature in the inner jet; the rotation measure of this feature ($\simeq 1300$ rad m^{-2}) agrees with the known high rotation measure of the source. The observations provide direct measurements of the rotation measure in the feature for which polarization was detected, making it possible to derotate the observed polarization vectors to infer the underlying magnetic field structure. This structure is roughly transverse to what appears to be the dominant flow direction, suggesting that this bright feature is associated with a relativistic shock.

Key words: radio continuum: galaxies – galaxies: jets – polarization – galaxies: magnetic fields – galaxies: quasars: individual: 3C 147

1. Introduction

The class of radio sources known as compact steep spectrum (CSS) sources has been discussed by many authors (e.g. Fanti et al. 1990; O'Dea 1998). They are loosely defined to have subgalactic dimensions and steep radio spectral indices ($\alpha \geq 0.5$ where $S_\nu \propto \nu^{-\alpha}$). It is now generally believed that most CSS sources are "young" radio sources whose lobes have not had time to expand to kiloparsec scales (Phillips & Mutel 1982; Fanti et al. 1990, 1995, for example). However, it seems likely that the structures and sizes of a sizeable minority of CSS sources result from interactions with dense ambient gas in the central regions of the parent optical objects, which confines the jets to the nuclear region and prevents them from forming the large-scale structure often observed in classical radio galaxies (Wilkinson et al. 1984, van Breugel et al. 1984, for example).

The bright quasar 3C 147 (0538+498) is a prominent CSS source at a redshift of $z = 0.545$. As a typical CSS source, 3C 147 has been observed by several investigators; see, for example, the 5-GHz MERLIN maps by Akujor et al. (1990) and Lüdke et al. (1998), the 8.4 and 15-GHz VLA maps of Akujor et al. (1995), and the VLBI map of Alef et al. (1990). The source has a complex structure with a well-resolved jet. The superluminal separation of two components in the inner jet has been observed (Alef et al. 1988). The inner part of the extended, well collimated jet is embedded in a region of more diffuse emission, and the jet bends sharply to the north roughly 200 mas from the core as it fades out (Mantovani et al. 1998).

Using the 45-m telescope at Nobeyama, Kato et al. (1987) and Inoue et al. (1995) measured a very large integrated rotation measure for 3C 147 (RM $\simeq 1500$ rad m^{-2}), suggesting that the radio source may be surrounded by a dense medium. If this is the case, the jet could be strongly interacting with the medium as it propagates through it. Knowledge of the geometry and degree of order of the magnetic field on milliarcsecond (mas) scales is critically important for estimating the physical conditions in the jet, understanding the energy transportation process, and analyzing the interactions between the jet and its environment.

By observing simultaneously at four different wavelengths in the 5-GHz band with the VLBA, we were able to image the distribution of polarization on mas scales and search for a λ^2 dependence for the polarization position angles (characteristic of Faraday rotation), in order to derive the distribution of RM across the VLBI source. This is important first and foremost because knowledge of the mas-scale RM is essential if we are to properly "derotate" the observed VLBI polarization vectors to infer the direction of the underlying magnetic field. If the integrated RM is associated with a foreground screen (in our Galaxy or near the source) that is uniform over the entire source emission region, it is sufficient to simply apply the integrated RM to derotate the observed polarization vectors. However, in the absence of VLBI polarization measurements, it is impossible to know whether the RM is completely associated with a uniform

Send offprint requests to: R.D. Nan

foreground screen or whether it is partially or fully associated with thermal plasma that is local to the source.

In the latter case, the mas-scale RM distribution could be very non-uniform, as was found for 3C119 (Nan et al. 1999). VLBI RM measurements can potentially allow us to identify RM gradients or regions of especially high RM on parsec scales. The distribution of RM in the source will reveal the structure of the medium causing the Faraday rotation. In the case of 3C 147, such information could help improve our understanding of the complex radio structure.

2. Observations and data reduction

2.1. Observations and data reduction

We observed 3C 147 for about 12 hours at 5 GHz with the VLBA in May 1995. The long synthesis time helped us to detect low-surface-brightness flux density. In general, it is quite difficult to reconstruct images in which there is are bright compact features embedded in much more extended emission. The abundance of short spacings in the VLBA u–v coverage was very useful in this respect, and we believe we have been able to reproduce the general features of the source structure reasonably reliably. Eight baseband converters (BBCs) were used, with four recording right-circular polarization and four left-circular polarization. Each BBC corresponded to 8 MHz of bandwith recorded with 1-bit sampling. The sky frequencies for the four BBCs (per polarization) were placed at four separate frequencies across the available 5-GHz band, which encompasses roughly 500 MHz; IFs 1–4 recorded 4650, 4845, 4853, and 5052 MHz, respectively. This enabled us to obtain truly simultaneous polarization images at these four frequencies. The observations were aimed at studying the rotation measure distribution on milliarcsecond scales. Due to technical limitations of the VLBA and BBC distribution system, it was not possible to set the BBCs to observe at four arbitrary frequencies, so that the four sky frequencies observed are not spread uniformly in the available band.

The data were calibrated, imaged, and analyzed using the AIPS package. During the reduction process, the data at each of the four separate frequencies were processed separately. The compact polarized source 0735+178 was used to determine the instrumental polarizations ("D-terms") using a linear approximation in the AIPS task LPCAL. The solution shows that the instrumental polarizations were typically of the order of 1%.

After the D-term calibration, there remains an arbitrary offset in the polarization position angles χ, which can be determined using data for a source in which a high fraction of the integrated polarization is present on mas scales. The usual method is to compare the integrated value of χ at the epoch of the VLBI observations with χ for the sum of the polarized flux on milliarcsecond scales, and rotate the VLBI χ values so that they agree with the integrated measurements. 0735+178 was used for this purpose as well. We used 5 GHz data for 0735+178 from the University of Michigan Radio Astronomy Observatory database (http://www.astro.lsa.umich.edu:80/obs/radiotel/radiotel.html) to estimate the integrated polarization position angle. The Michigan measurements were separated from the VLBI epoch by six days; although substantial polarization variations can occur in compact AGN on this time scale, other Michigan polarization measurements before and after our VLBA observations suggest that the 5 GHz χ value was relatively stable in this period, so that we believe that the time interval between the Michigan and VLBA observations has not introduced a large error into our absolute χ calibration. In order to remove any offsets between frequencies, we first rotated the phases of the polarisation uv data for all the sources so that the χ values for 0735+178 at each of the four frequencies were aligned with the value in IF 1. This assumes that the Faraday rotation of 0735+178 across the observed bandwidth is negligible; this is a reasonable assumption, given the low integrated rotation measure of this source (10 rad m^{-2}; Rudnick & Jones 1983). We then estimated the polarization of 0735+178 on mas scales from the sum of its Q and U flux densities.

As an overall check of the reliability of our calibration, we made images for 0735+178 separately for each of the four IFs. The resulting four I and P images were similar to each other even in details, giving us confidence in our inter-IF and D-term calibration.

A data cube for 3C 147 at our four observing frequencies was obtained using the AIPS task MCUBE. We then mapped the rotation-measure distribution using the AIPS task RM, which performs a weighted fit of the position angle to the λ^2 dependence expected for Faraday rotation. Finally, the intrinsic magnetic-field vectors were obtained by using the RM results to "derotate" the observed χ values for the VLBI polarization distribution.

3. Results

3.1. Total intensity images

The total intensity (*I*) image obtained using all four IFs is shown in Fig. 1; this image has an angular resolution of 2.8×2.5 mas. The rms noise level on this image (determined by considering areas without any source emission) is about 0.22 mJy, just over a factor of two higher than the noise level expected theoretically. Since the theoretical thermal noise limit is rarely reached even in the best images, this rms noise level is about what we would expect. In the presence of very well calibrated data, this would normally lead us to expect obviously spurious features to begin to appear at roughly the 3σ level, or about 0.66 mJy/beam; in contrast, the bottom contour on our image, at which small unphysical features begin to appear in the core region, is about 1.48 mJy/beam, roughly twice this expected value. This suggests the presence of minor but significant residual calibration errors, probably due to the difficulty in imaging complex structures having both compact features and very extended emission. However, we emphasize that this does not affect our interpretation of our images, since we are primarily interested in the general location of the polarized emission in the source and its wavelength dependence, not in details of the source structure. As discussed below, our *I* image is in good qualitative agreement with those made in other studies.

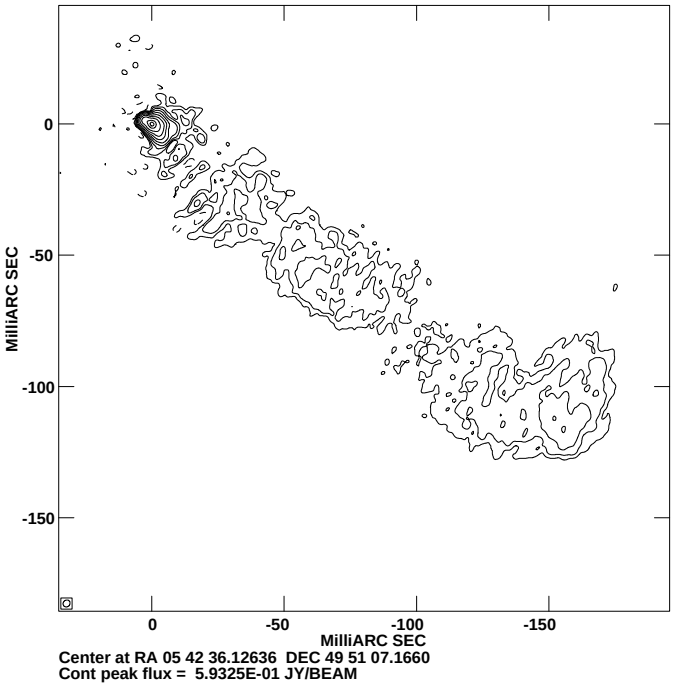

Fig. 1. VLBI total intensity (*I*) image of 3C 147 made using all of our four observing frequencies. The contours are -0.25, 0.25, 0.5, 1, 2, 4, 8, 16, 32, 64, and 90% of the peak brightness of 0.593 Jy/beam.

We also made *I* images for each of the four individual IFs, which are very similar to Fig. 1, with the expected rise of about a factor of two in the noise level. The total flux density in the image in Fig. 1 is $\simeq 4.4$ Jy, which is slightly more than half the single-dish flux (Dallacasa & Stanghellini 1990). Thus, a large fraction of the flux density has been resolved out by the VLBI baselines, even though our images follow the jet to a distance of about 200 mas. The observed structure can be divided into two parts: the complex core region (head of the jet) and the more or less collimated jet, which has a rather small opening angle. We can also see possible gentle wiggling from the head to the end of the detectable jet, where the jet bends sharply (through roughly 90°) toward the northwest. The main spine of the jet emerges from the core and connects smoothly with the jet emission on scales of tens of mas. However, there is more complex emission surrounding the inner jet, within about 10 mas from the core.

3.2. Complex core region

Fig. 2 shows a close-up of the core region for our image at one of the IFs (frequency 4845 MHz). This image is dominated by two compact components embedded in more diffuse emission: one at the position of the peak (component B) and one to the northeast of the peak (component A). There is also more extended emission in this region, dominated by bulges toward the northwest and west. It is difficult to judge the reality of this emission based on our image alone; however, rather similar structures are present in the images of Alef et al. (1988, 1990), which were obtained with completely different VLB arrays, suggesting that these extended emission features are probably real.

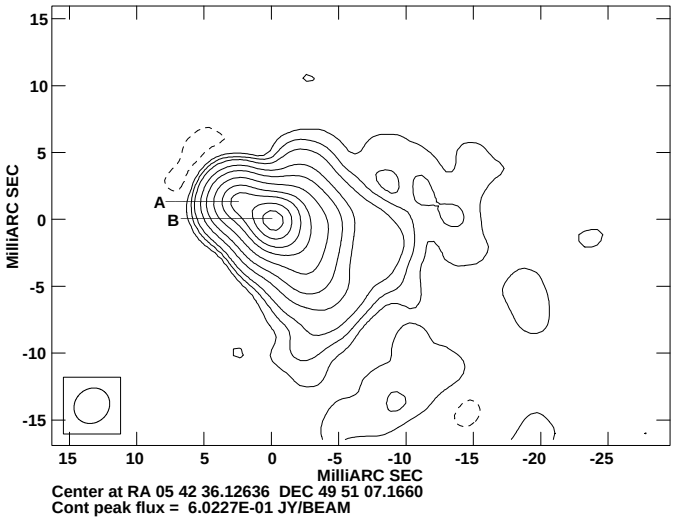

Fig. 2. Close-up VLBI total intensity (*I*) image of the core region of 3C 147 at one of four the IFs (frequency 4845 MHz). The contours are -0.4, 0.4, 1, 2, 5, 10, 20, 35, 50, 70, and 90% of the peak brightness of 0.602 Jy/beam.

Table 1. Total flux densities for VLBI components in 3C 147

IF	ν (MHz)	Component	S(Jy)
1	4650	A	0.34
		B	1.50
2	4845	A	0.37
		B	1.53
3	4853	A	0.36
		B	1.53
4	5052	A	0.34
		B	1.50

The total densities of component A and B were obtained by summing the flux density corresponding to the components using the AIPS task IMSTAT. The results are listed in Table 1; we can see that the flux densities of A and B do not show any obvious frequency dependence within our observing band. We identify the northeast component as the core, based on its relatively weak polarization (see Sect. 3.3). The peak corresponds to a bright knot in the jet. The connection between this brightening of the jet and the more diffuse emission in this region is not clear, although it is tempting to suppose that they are related.

In a maximum-entropy image of the core region with resolution 1×1 mas derived using the AIPS task VTESS (Fig. 3), we can see more distinctly the two components referred to above: the northeast core (A) and the southwest jet knot (B). The positions of the components are marked in Fig. 3. Using our own data together with the earlier observations (Alef et al. 1990), we confirm superluminal motion between A and B at an apparent speed $\beta \simeq 1.5c$ ($H_0 = 100$ km s^{-1}Mpc^{-1}; $q_0 = 0.5$); the spacing between A and B increased by about 1.2 mas from August 1984 to May 1995. The apparent velocity we have derived ($\beta \simeq 1.5c$) is very similar to that found by Alef et al. (1990) for this same feature ($\beta \simeq 1.3c$).

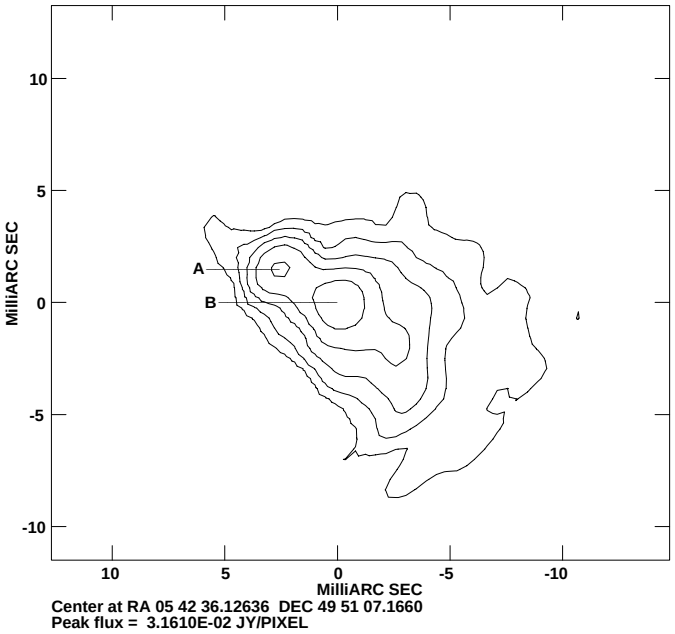

Fig. 3. Super-resolved *I* map of the core region of 3C 147 at the same frequency shown in Fig. 2 (4845 MHz). The contours are −1.0, 1, 3, 8, 20, and 50% of the peak brightness of 0.0316 Jy/pixel.

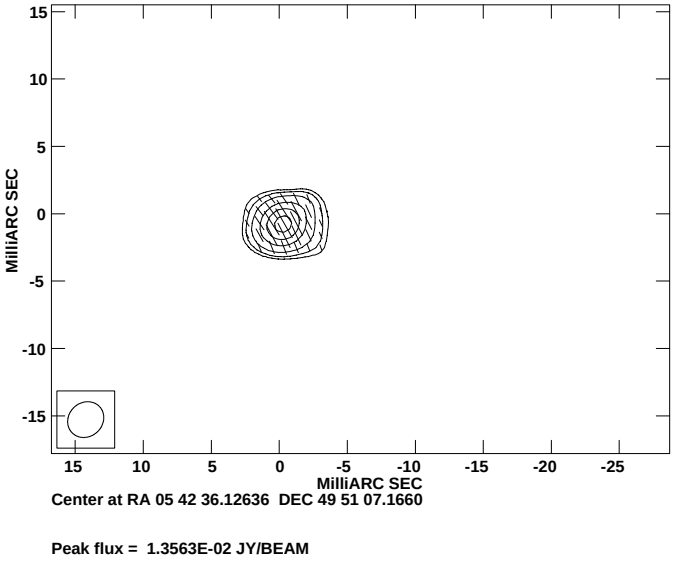

Fig. 4. Superposition of χ sticks and linearly polarized flux density (*p*) for 3C 147 at the same frequency as Fig. 2 (4845 MHz). The *p* contours are 15, 20, 30, 50, 70, and 90% of the peak brightness of 13.6 mJy/beam.

3.3. Linear polarization

Polarization was detected only in the region of the bright jet component B. The upper limit to the polarization of component A is about 1.5 mJy, or about 0.5%. The polarized intensity distribution of 3C 147 for IF 2 is shown in Fig. 4 with contours of polarized intensity and χ sticks superimposed.

Fig. 5 shows a superposition of the contour map of *I* shown in Fig. 2 and a grey-scale map of the polarized flux density p

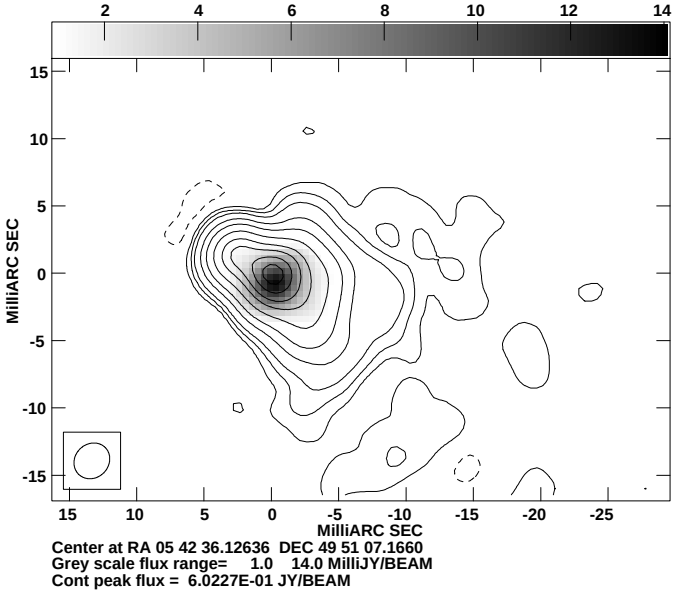

Fig. 5. Superposition of linearly polarized flux density(*p*) and total intensity(*I*) images for 3C 147 at the same frequency as Fig. 2 (4845 MHz). The contours are −0.4, 0.4,, 1, 2, 5, 10, 20, 35, 50, 70, and 90% of the peak brightness of 0.602 Jy/beam. The polarized flux density grey scale ranges from 1.0 to 14.0 mJy/beam.

Table 2. Polarization parameters of component B in 3C 147

IF	ν (MHz)	p (mJy)	χ (deg)	m (%)
1	4650	15	5.5	1.96
2	4845	16	30.6	2.01
3	4853	16	31.0	2.03
4	5052	14	52.8	1.89

in the same region at the same frequency. The polarizations of B at the four frequencies are listed in Table 2. In principle, our four images have slightly different resolutions, since they correspond to slightly different frequencies; the largest frequency (resolution) difference is about 10%. The polarization maps for the four different frequencies are all very similar, indicating that this effect was not appreciable for these images. The polarizations in Table 2 were determined by summing the total Q and U fluxes for component B in each image, so that the slight differences in the resolutions of the images were accounted for. We estimated the total complex polarization on VLBI scales from the total flux densities on the Q and U maps to be about 20 mJy, nearly all in component B. The integrated 5-GHz polarized flux density from the University of Michigan Radio Astronomy Observatory measurements is also roughly 20 mJy, indicating that essentially all the integrated polarized flux is present on our VLBI image.

The overall degree of polarization of B is about 2.0% (Table 2). We can see from the linearly polarized flux density map in Fig. 5 that the *p* peak is shifted about 1 mas to the south from the *I* peak. The origin of this offset is not clear, since it has no obvious relation to the direction of either the jet or the more diffuse structure near the core. In principle, it is larger than we

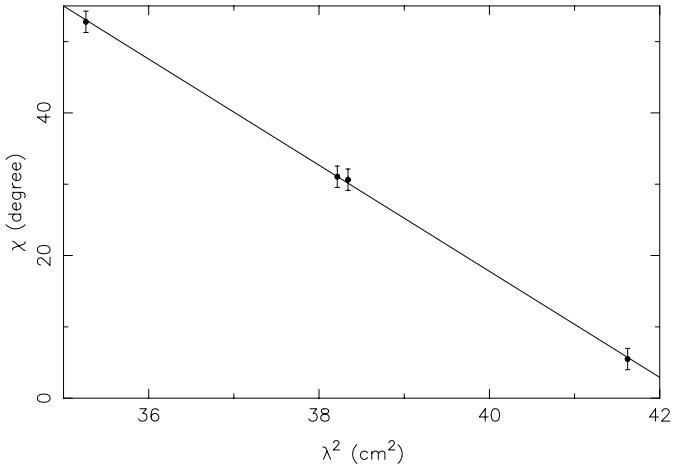

Fig. 6. Plot of the observed χ values for the polarizations of component B as a function of λ^2 for the four wavelengths at which we observed.

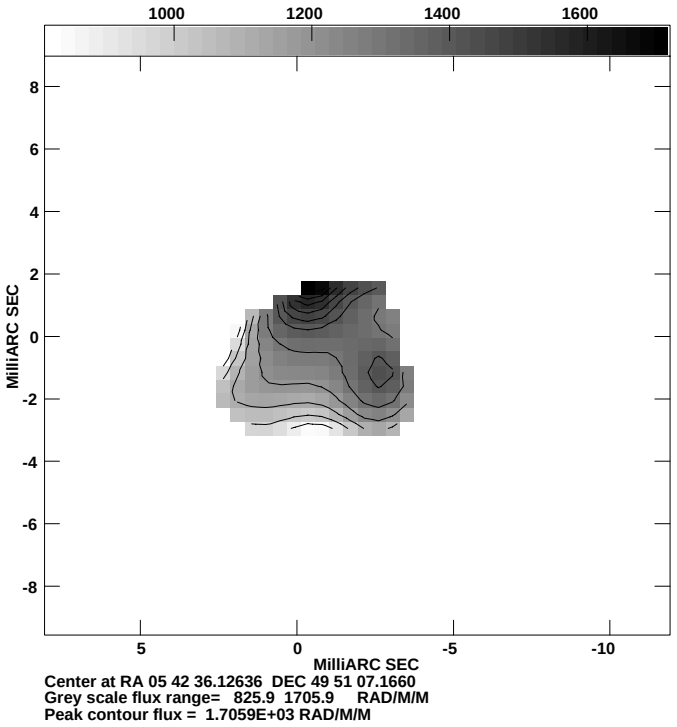

Fig. 7. Rotation Measure distribution in the core region where the formal uncertainty in the local rotation measure is less than ± 100 rad m^{-2}. The contours correspond to rotation measures of 800, 900, 1000, 1100, 1200, 1300, 1400, 1450, 1500, 1550, 1600, 1650, and 1700 rad/m^2. The grey scale ranges from 825.9 to 1705.9 rad/m^2. The actual value of the RM is the negative of that in the figure.

would expect if it were associated with residual calibration errors (Roberts et al. 1994); in addition, our polarization images of 0735+178 gave no indication of calibration problems. We therefore believe that this offset is likely real, but higher-resolution observations are required to reveal its origin.

3.4. Rotation measure structure and intrinsic magnetic fields

Fig. 6 shows the χ values for component B at each of the four frequencies plotted as a function of λ^2. We used the χ values at the *p* peaks of the four *p* maps to estimate the RM for component B. The uncertainty of the χ values in Fig. 6 was determined by comparing the χ values for IF 2 and IF 3, which corresponded to nearly the same frequencies. The implied errors in χ are about $\pm 0.5^\circ$. The errors shown in Fig. 6 are 3σ. If the variations of χ with wavelength are associated with Faraday rotation, we expect the χ values to form a straight line in this plot. We can see that the χ variations for component B can be described well by a λ^2 dependence, indicating the presence of Faraday rotation; the best linear fit to the data in Fig. 6 yields a RM for component B of 1300 ± 30 rad m^{-2}.

Fig. 7 shows the rotation measures calculated from the four-frequency data on a pixel-by-pixel basis with a blanking error of ± 100 rad m^{-2} as a contour map with a superposed grey scale; Fig. 8 shows the same grey-scale RM distribution superposed on the total-intensity contours. No redshift corrections have been applied to the wavelengths, so the RMs in the rest frame of 3C 147 are larger by a factor of $(1+z)^2$. The RM distributions in Figs. 7 and 8 range from -1700 to -800 rad m^{-2}, with the value near the peak of the polarization map being about -1300 rad m^{-2}, similar to the value for component B as a whole indicated by the plot in Fig. 6. The RM distribution does not show any obvious smooth gradients of the sort found in component C of 3C119 (Nan et al. 1999), and though there are formally regions of higher rotation measure offset from the *p* peak, these have no obvious relation to the source structure. Therefore, we conclude that the resolution and sensitivity of our measurements were sufficient to verify that the rotation measure in the region of component B is close to the integrated value determined by Kato et al. (1990) (-1500 rad m^{-2}), but not to map out more detailed structure in the RM distribution on parsec scales.

Based on the lack of clear evidence for structure in the distributions of polarization and rotation measure, we decided to apply a single rotation to account for the RM detected for component B. The inferred projected magnetic field configuration for 3C 147, corrected for the rotation measure, is shown in Fig. 9. The **B** vectors are oriented roughly transverse to the direction along the spine of the jet, suggesting that the bright component B may be associated with a shocked region.

4. Discussion

VLA observations of dominant members of luminous X-ray clusters with large cooling flows (e.g., Cyg A) show that very high rotation measures can be produced by a medium located (1) within the source itself; (2) in a thin sheath surrounding the source; or (3) in the hot, X-ray emitting gas of the intergalactic medium. Considering 3C 147's Galactic latitude (10.3°), where typical Galactic rotation measures are tens of rad m^{-2}, the Galactic contribution to the RM of 3C 147 is likely to be negligible (Kato et al. 1987). Since our observations do not detect significant depolarization (Table 2), the large rotation measure

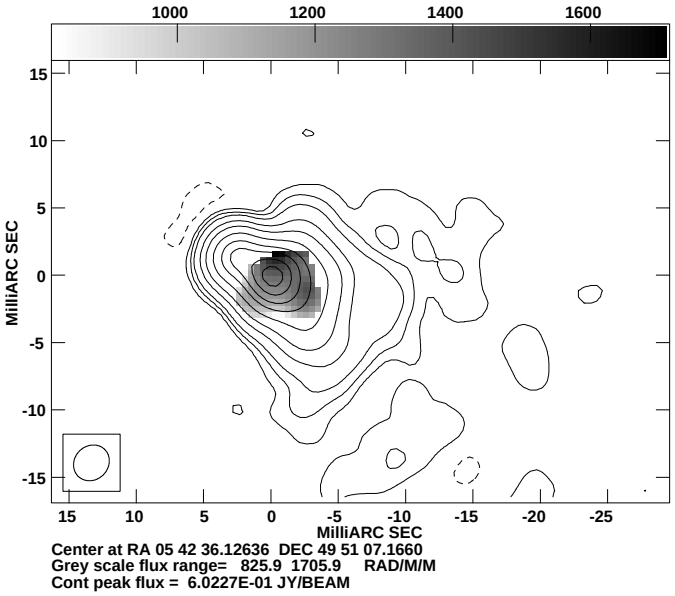

Fig. 8. The same total intensity contours shown in Fig. 2, superposed with the rotation-measure distribution in the core region at pixels where the formal uncertainty in the local RM is less than ± 100 rad m^{-2}. The actual value of RM is the negative of that in the figure.

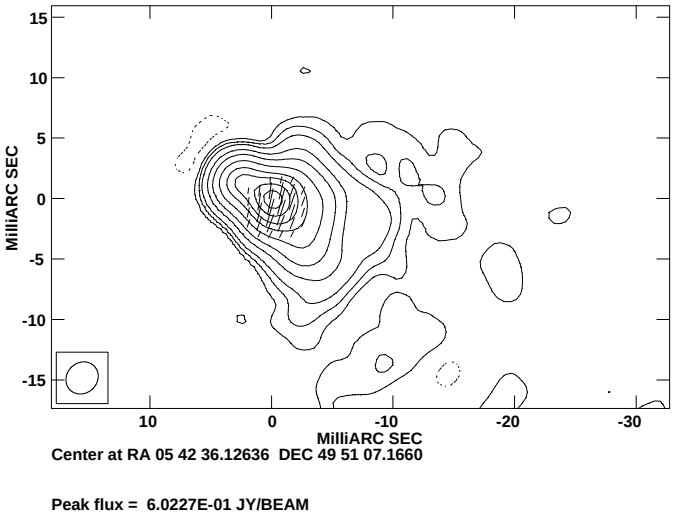

Fig. 9. The same total intensity contours shown in Fig. 2, with magnetic field vectors superposed. The intrinsic orientation of the **B** vectors was determined by "derotating" the observed χ values using the derived rotation measure for component B.

in 3C 147 may be due to some combination of mechanisms (2) and (3) operating on mas scales.

The rotation measure distribution in Figs. 7 and 8 suggests the possible presence of small-scale RM gradients, but the resolution and sensitivity of our observations were insufficient to reliably detect such gradients. If subsequent observations convincingly demonstrate the presence of RM gradients in component B, this will probably rule out an origin of the RM within the surrounding cluster gas (Dreher et al. 1987).

In the CSS source 3C119, Nan et al. (1999) showed that the thermal plasma associated with the observed Faraday rotation was localized in the vicinity of the bright component C, which was located at a sharp bend in the VLBI jet. A RM gradient along the direction of the jet flow into component C was detected. Nan et al. (1999) concluded that the Faraday rotation was associated with a dense cloud of thermal plasma with which the jet had collided, sharply deflecting the jet. In the case of 3C 147, the situation is different: the jet continues far beyond component B, with very little change in direction. The jet appears to be quite well collimated beyond component B, and shows only gentle wiggles until the sharp bend observed about 200 mas from the core. This argues against a scenario such as that in 3C119, where there was a localized concentration of thermal plasma that strongly deflected the VLBI jet. At the same time, the fact that the surface brightness of the VLBI jet decreases beyond component B may suggest some interaction between the jet and surrounding medium in the region of B. Given the available evidence, it is perhaps most likely that the Faraday rotating plasma in 3C 147 is associated with a cocoon surrounding the jet. The cocoon plasma may be densest in the inner jet, leading to the brightness of the region near component B and the lower surface brightness of the jet further from the core.

5. Conclusion

With our milliarcsecond-resolution observations, we have been able to confirm the presence of high RMs consistent with the integrated measurements in the inner jet component B, which was the only component in which polarization was detected. The observations at the four frequencies were simultaneous, and have enabled us to derive information about the distribution of the rotation-measure of 3C 147 on parsec scales.

The VLBI total intensity structure of 3C 147 at 5 GHz shows the core and a jet extending to the southwest in position angle $\simeq -130°$. The peak of the polarization distribution is displaced about 1 mas to the south of the *I* peak; the origin of this is not clear, and higher resolution observations are needed to investigate this question.

The rotation measure in the vicinity of component B formally ranges from -1700 to -800 rad m^{-2}, taking on its largest magnitude about 1 mas to the north of the *I* peak. However, this formal RM distribution has no obvious relation to the *I* or *p* structure, and we believe that the extremes of the observed range of rotation measures, which occur far from both the *I* and *p* peaks, are random fluctuations due to the larger uncertainties in the polarization position angles in these regions, which have relatively poorly determined polarizations. We conclude that our observations have allowed us to measure the average local rotation measure for component B (1300 ± 30 rad m^{-2}), but not to reliably detect structure in the RM distribution.

Nonetheless, the fact that we did not detect any large rotation measure gradients suggests that the situation in 3C 147 differs from that in 3C119, in which there was a very large RM gradient along the jet direction, across a bright component at a very sharp bend in the jet. It seems likely that the Faraday rotat-

ing material in 3C 147 is less concentrated than in 3C119, and may be associated with a cocoon or sheath of thermal plasma surrounding the jet. Further higher resolution observations are required to test this possibility.

The magnetic field in component B inferred after "derotation" using the observed mas-scale rotation measure is transverse to the jet direction, suggesting that this bright feature may be associated with a shocked region.

Acknowledgements. RDN is supported by a grant from the National Natural Science Foundation in China. He thanks the NAO of Japan for hospitality during his visit, and Dr. Carlo Stanghellini for his useful suggestions. DCG acknowledges support from the European Commission under TMR contract No. ERBFMGECT950012. The National Radio Astronomy Observatory(NRAO) is a facility of the National Science Foundation operated under cooperative agreement by Associated Universities, Inc. This research has used the data from the University of Michigan Radio Astronomy Observatory which is supported by funds from the University of Michigan. Finally, we would like to thank the anonymous referee for his careful and conscientious review of the manuscript.

References

Akujor C.E., Spencer R.E., Wilkinson P.N., 1990, MN 244, 362
Akujor C.E., Garrington S.T., 1995, A&AS 112, 235
Alef W., Preuss E., Kellermann K.I., Whyborn N., Wilkinson P.N., 1988, In: Reid M.J., Moran J. M. (eds.) IAU Symp.129, The Impact of VLBI in Astrophysics and Geophysics. Kluwer, Dordrecht, p. 95
Alef W., Preuss E., Kellermann K.I., 1990, In: Fanti C., et al. (eds.) Compact Steep Spectrum & GHz-Peaked Spectrum Radio Sources. CNR, Bologna, p. 149
Dallacasa D., Stanghellini C., 1990, In: Fanti C., et al. (eds.) Compact Steep Spectrum & GHz-Peaked Spectrum Radio Sources. CNR, Bologna, p. 224
Dreher J.W., Carilli C.L., Perley R.A., 1987, ApJ 316, 611
Fanti R., Fanti C., Schilizzi R.T., et al., 1990, A&A 231, 333
Fanti C., Fanti R., Dallacasa D., et al., 1995, A&A 302, 317
Inoue M., Tabara H., Kato T., Aizu K., 1995, PASJ 47, 725
Kato T., Tabara H., Inoue M., Aizu K., 1987, Nat 329, 223
Lüdke E., Garrington S.T., Spencer R.E., 1998, MN 299, 467
Mantovani F., Junor W., Bondi M., et al., 1998, A&A 332, 10
Nan R.D., Gabuzda D., Kameno S., Schilizzi R.T., Inoue M., 1999, A&A 344, 402
O'Dea C.P., 1998, PASP 110, 493
Phillips R.B., Mutel R.L., 1982, A&A 106, 21
Roberts D.H., Wardle J.F.C., Brown L.F., 1994, ApJ 427, 718
Rudnick L., Jones T.W., 1983, AJ 88, 518
van Breugel W., Miley G., Heckman T., 1984, AJ 89, 5
Wilkinson P.N., Booth R.S., Cornwell T.J., Clark R.R., 1984, Nat 308, 619